Research Article

Patthranit Wongpromrat, Phacharaphon Tunthawiroon, Eakarach Bumrungthaichaichan, Phisan Ponpo, Thanasak Nilsonthi, Somrerk Chandra-ambhorn*, and Walairat Chandra-ambhorn

Possibility of metallic cobalt formation in the oxide scale during high-temperature oxidation of Co-27Cr-6Mo alloy in air

https://doi.org/10.1515/htmp-2022-0302 received June 09, 2023; accepted November 24, 2023

Abstract: Co-based alloys are known to be high oxidation-resistant material and used in several high temperature applications. During high temperature oxidation, duplex oxides containing Co and Cr were formed. It was thermodynamically elucidated that when the growing scale was thick enough, the partial pressure of O_2 in the scale dropped. Then, the reduction of CoO occurred for promoting O_2 which was responsible for Cr_2O_3 production.

This work experimentally proved this point by *in situ* characterising Co-27Cr-6Mo at high temperatures in air by X-ray diffractometer in a grazing incident mode and metallic Co was confirmed to be formed by the reduction of CoO consistent with the image taken and analysed by field emission scanning electron microscope, energy-dispersive X-ray, and electron backscatter diffraction. Furthermore, the change in lattice parameter and the phase transition were observed when the temperature was altered.

Keywords: CoO reduction, co-based alloy, *in situ* characterisation, high temperature oxidation, oxide scale evolution

* Corresponding author: Somrerk Chandra-ambhorn, High Temperature Corrosion Research Centre, Department of Materials and Production Technology Engineering, Faculty of Engineering, King Mongkut's University of Technology North Bangkok, 1518 Pracharat 1 Road, Wongsawang, Bangsue, Bangkok, 10800 Thailand, e-mail: somrerk.c@eng.kmutnb.ac.th

Patthranit Wongpromrat: Department of Chemical Engineering, School of Engineering, King Mongkut's Institute of Technology Ladkrabang, 1 Soi Chalongkrung 1, Ladkrabang, Bangkok, 10520, Thailand, e-mail: patthranit.wo@kmitl.ac.th

Phacharaphon Tunthawiroon: Department of Industrial Engineering, School of Engineering, King Mongkut's Institute of Technology Ladkrabang, 1 Soi Chalongkrung 1, Ladkrabang, Bangkok, 10520, Thailand, e-mail: phacharaphon.tu@kmitl.ac.th

Eakarach Bumrungthaichaichan: Department of Chemical Engineering, School of Engineering, King Mongkut's Institute of Technology Ladkrabang, 1 Soi Chalongkrung 1, Ladkrabang, Bangkok, 10520, Thailand, e-mail: eakarach.bu@kmitl.ac.th

Phisan Ponpo: Department of Chemical Engineering, School of Engineering, King Mongkut's Institute of Technology Ladkrabang, 1 Soi Chalongkrung 1, Ladkrabang, Bangkok, 10520, Thailand, e-mail: phisan.po@kmitl.ac.th

Thanasak Nilsonthi: High Temperature Corrosion Research Centre, Department of Materials and Production Technology Engineering, Faculty of Engineering, King Mongkut's University of Technology North Bangkok, 1518 Pracharat 1 Road, Wongsawang, Bangsue, Bangkok, 10800 Thailand, e-mail: thanasak.n@eng.kmutnb.ac.th

Walairat Chandra-ambhorn: Department of Chemical Engineering, School of Engineering, King Mongkut's Institute of Technology Ladkrabang, 1 Soi Chalongkrung 1, Ladkrabang, Bangkok, 10520, Thailand, e-mail: walairat.ch@kmitl.ac.th

1 Introduction

Co-based alloys are the materials preferred to be used at high temperatures. The objective of designing these materials is primarily for improving the mechanical properties at elevated temperatures [1–3]. They are used in various engineering applications, such as in combustion chamber in gas turbine, nuclear power plants, and die casting processes [1,4–6]. Several elements are usually added to Co-based alloy for enhancing some properties, e.g. Cr is usually alloyed with higher content than 20 wt% to improve the oxidation resistance [1]. One of the most common compositions compounded is CoCrMo alloy.

The high temperature oxidation of CoCrMo alloys has been studied for several years by the *ex situ* demonstrations and characterisations by various techniques. Kofstad and Hed [7–9] were the first who oxidised Co-25Cr and Co-10Cr at high temperatures in various O₂ partial pressures and their kinetics and scale formed were studied. After that, there were many researches trying to improve the properties, especially for high temperature oxidation resistance, of Co-based alloys by alloying with other elements [10–12] including with the work of Li et al. [5]. They oxidised Co-29Cr-6Mo in air at 700°C and reported that CoO was first formed on the specimen. The growing scale led to the decrease in O₂ partial pressure in

the oxide layer, then the reduction of CoO by Cr occurred promoting the O that was responsible for Cr₂O₃ production, and the byproduct obtained was the metallic Co. This hypotheses seemed to be in good agreement with Ellingham diagram and the work of Young et al. [13] proving that the partial pressure of O₂ inside the oxide scale was expected to be much lower than that in the air as a result of the extremely low diffusion coefficient of O atoms through the oxide scale. Moreover, from our latest study [14], the metallic Co can be observed in the oxide scale after high temperature oxidation of Co-27Cr-6Mo alloy characterised by field emission scanning electron microscope (FESEM) and energy-dispersive X-ray (EDX). The reduction of CoO to form the metallic Co is disadvantage and should be avoided because, from our previous study [14], Co can volatilise at higher oxidation rate than that of CoO about three orders of magnitude at 900 and 1,000°C leading to the loss of Co element and increase in Cr2O3 thickness. The effect of Co volatilisation, rather than the loss of Co element, has been unknown at the present since this phenomenon has just been found and needed further studies to elucidate. For Cr₂O₃ formation, it is well known that it helps improve the oxidation resistance [15–17] since it is a protective oxide layer, so it acts as a diffusion barrier protecting the further oxidation of the matrix element [16] and, thus, the degradation is decelerated. Nevertheless, the thickening Cr₂O₃ develops the stress in the oxide and the cracks may occur after a long exposure [18]. In addition, Cr₂O₃ formation leads to poorer electrical conductivity of the alloys compared to the base-alloy [19,20] and Cr₂O₃ can volatilise when exposed to O2, and further aggressive rate in the presence of H2O [21], at high temperatures resulting in the loss of protective layer, then the poorer oxidation resistance. These disadvantages are not good especially when it is used as a metallic interconnect of solid oxide fuel cells (SOFCs) because high electrical resistance is needed and the Cr-volatile species causes a Cr-poisoning of the cathode material leading to worse potential of SOFCs [22].

In this work, this CoO reduction situation was proved again by using *in situ* technique. The Co-27Cr-6Mo alloy was oxidised in air at high temperatures in X-ray diffractometer (XRD) where the *in situ* characterisations were carried out to observe the phases formed on the specimen in the different stages of oxidation.

2 Experimental procedures

2.1 Materials preparation

Co-27Cr-6Mo alloy, with the chemical composition given in Table 1, was supplied by Eiwa Co., Ltd. (Japan) as a

Table 1: Chemical composition of Co-26Cr-6Mo alloy used in this work

| Element | Cr | Мо | С | Si | Mn | Со |
|---------|-------|------|------|------|------|------|
| wt% | 26.70 | 5.90 | 0.04 | 0.61 | 0.45 | Bal. |

cylindrical bar with the diameter of 25 mm. Then, it was cut into 2 mm thick. Prior to the high temperature oxidation experiments, the specimens were polished by SiC paper, finished by 1- and 0.3-µm alpha alumina suspension (AP-A suspension, Struers), and cleaned with ethanol in an ultrasonic bath at 60°C for 15 min.

2.2 Oxidation kinetics

The high temperature oxidation experiments of the specimens were performed in the muffle furnace in the atmospheric air. The temperature was constantly controlled at 900°C for 24, 48, 72, and 96 h with the heating rate of $15^{\circ}\text{C}\cdot\text{min}^{-1}$. The weights of the specimens were measured by using a 4-digit balance with the sensitivity of 10 μg before and after the experiments to observe the weight changes during oxidation.

2.3 Material characterisations

The in situ characterisations of specimens were achieved in the X-ray diffraction spectroscopy (SmartLab-Rigaku) in the grazing incident mode (GI-XRD) under high temperatures because the oxide films developed during an early stage of oxidation were supposed to be thin. There were three specimens in this study: Specimen A oxidised at 900°C, Specimen B oxidised at 1,000°C, and Specimen C characterised at 900 and 1,000°C, subsequently. For Specimens A and B, the in situ characterisations were made four times per specimen. The first time of characterisations on both specimens was at 30°C (room temperature) giving the results A1 and B1 for Specimens A and B, respectively. After that Specimens A and B were heated up to the desired temperatures of 900 and 1,000°C, respectively, with the heating rate of 15°C·min⁻¹. The second characterisations were made after holding the specimens at the desired temperatures for 5 min and aligning the sample for 10 min giving the results A2 and B2. Then, the specimens were continuously held at the desired temperatures for 5 min. The third characterisations were achieved after the sample alignment for 10 min providing the results A3 and B3. Afterward, the specimens were

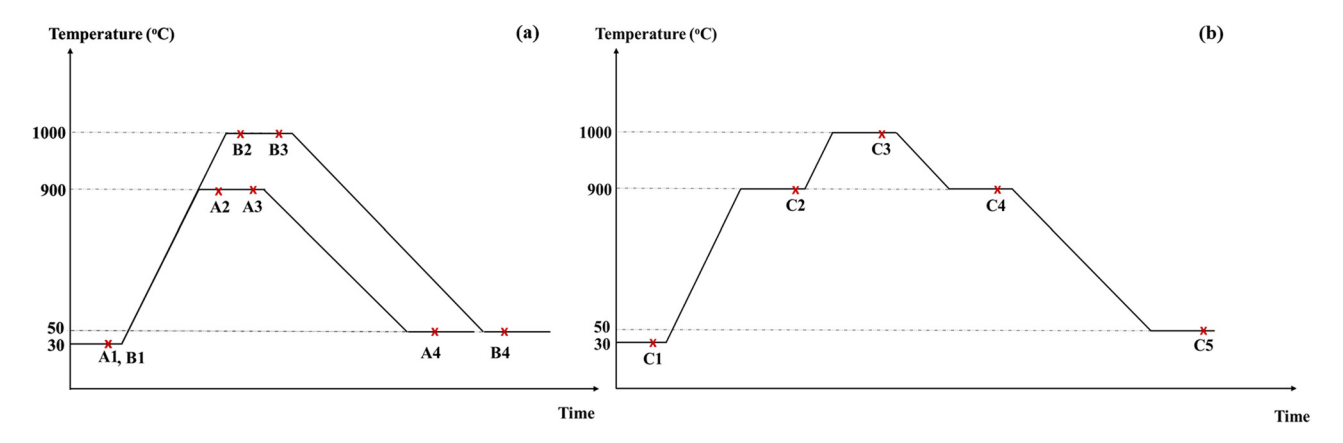


Figure 1: Experimental steps and the characterisation conditions during high temperature oxidation of (a) Specimens A and B and (b) Specimen C. The symbol "x" represents where the characterisation occurs.

cooled down at the rate of 30°C·min⁻¹ to 200°C. Then, the temperature dropped freely to 50°C without the use of air pressure pump (uncontrol rate) which was taken about 15 min. After holding at 50°C for 1 min and sample alignment for 10 min, the fourth characterisations, A4 and B4, were achieved. All characterisation steps of Specimens A and B are illustrated in Figure 1a.

Specimen C was double-step oxidised. The temperature was first increased to 900°C followed by 1,000°C to compare the oxide formed with that on the Specimens A and B which were the single-step oxidations. The *in situ* characterisations of this specimen were made five times (C1 to C5) as shown in Figure 1b. The results C1 to C3 were attained at 30, 900, and 1,000°C. From 1,000°C, the specimen was cooled down to 900°C where the fourth characterisation (C4) was achieved for observing the stability of the oxide formed on the specimen surface before cooling

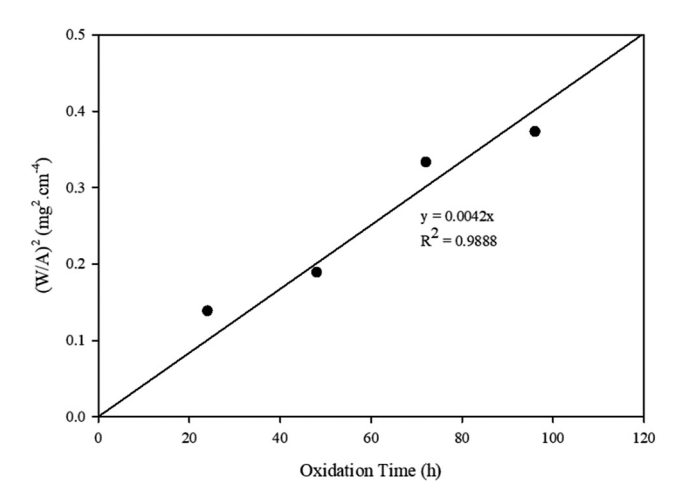


Figure 2: The square mass gain of Co-27Cr-6Mo oxidation in air at 900°C for 24–96 h.

down to 50°C at which the last characterisation occurred (C5). Similar to Specimens A and B, prior to shoot the X-ray for analysis, the specimen was held at the desired temperatures for 5 min followed by the sample alignment for 10 min. After *in situ* characterisations at high temperatures, the cross-sections of Specimens A, B, and C were prepared and characterised by FESEM-EDX (Apreo S-Thermo Fisher Scientific) and Electron Backscatter Diffraction (EBSD).

3 Results and discussion

3.1 Oxidation kinetics

Figure 2 shows that the square specific mass gains, $(W/A)^2$, during oxidation of Co-27Cr-6Mo alloy in air at 900°C were plotted against the oxidation time. From the graph, it can be seen that the square specific mass gain and time align the linear relation with the R^2 of 0.9888 implying that this was the parabolic oxidation according to equation (1) with the reaction rate constant of 4.20×10^{-3} mg²·cm⁻⁴·h⁻¹ and the oxides formed on the specimen surface were protective. Table 2 shows the comparison of kinetic rate constants

Table 2: Chemical composition of Co-26Cr-6Mo alloy used in this work

| Alloy | Kinetic constant (mg²·cm ^{–4} ·h ^{–1}) | Reference | | |
|--------------------------|--|--------------|--|--|
| Co-27Cr-6Mo | 4.20×10^{-3} 4.00×10^{-3} | This work | | |
| Co-25Cr Co-23Cr-11Ni- | 2.80×10^{-3} | [23] [24] | | |
| 7W-3Ta | | | | |

attained from this work and the literatures of Phalnikar et al. [23] and Hou [24] oxidising Co-based alloy in air at 900°C. It can be elucidated that our kinetic rate constant was comparable with that of the literatures especially for the oxidation constant of Phalnikar et al. [23] that oxidised the alloy containing rather close Cr content to this work. Considering the kinetic rate constant of Hou [24], it can be seen that our constant was little lower than that of Hou [24] even the Cr content in their alloy was lower. This was due to the Ni content in the alloy which was known to be the element promoting the oxidation resistance of the alloys.

$$\left(\frac{W}{A}\right)^2 = kt. \tag{1}$$

3.2 Oxide formation

FESEM and EDX were used to characterise the oxides formed on those three specimens after high temperature oxidation in air. The cross-sectional images and the cartoghaphies are shown in Figure 3. From all specimens, CoO can be obviously seen at the external layer of the oxide scale while Cr_2O_3 was internally grown at the metal/oxide interface. This related to many literatures [5,7,8,25,26] confirming the outward diffusion of Co^{2+} and the inward

diffusion of O. In addition, the Co was observed at the pointed position in the scale of Specimens A and B while O was absent in that place. This revealed that the metallic Co was actually formed in the oxide scale and the possible reaction is as in equation (2). For Specimen C, the large narrow area which seemed to be the crack can be observed in FESEM image. The EDX element map shows that it was an O-free area. However, Co and a little Cr could still be seen revealing that it was not the crack position. To go deeper, EBSD was used to characterise Specimen C and the results are shown in Figure 4. Figure 4a and b shows the images of the area including the scale and the matrix. This specified that the major phase formed in the scale was CoCr₂O₄. The metallic Co with the same phase (green area) as in the matrix was obviously seen in the oxide layer and the few amounts of Cr₂O₃ was distributed in the scale.

$$3C_{0}O + 2C_{r} \rightarrow 3C_{0} + C_{r_{2}}O_{3}.$$
 (2)

The oxide scale at the hole area which seemed to be the crack similar to what observed by FESEM in Figure 3 was focused and its EBSD images are displayed in Figure 4c and d. Since it was the hole, so the X-ray coming from the source and going inside the hole cannot diffracted back to the detector resulting in the black area in the image. Nevertheless, at the edge of this area Cr_2O_3 and Co ensuring that this area was not the crack position.

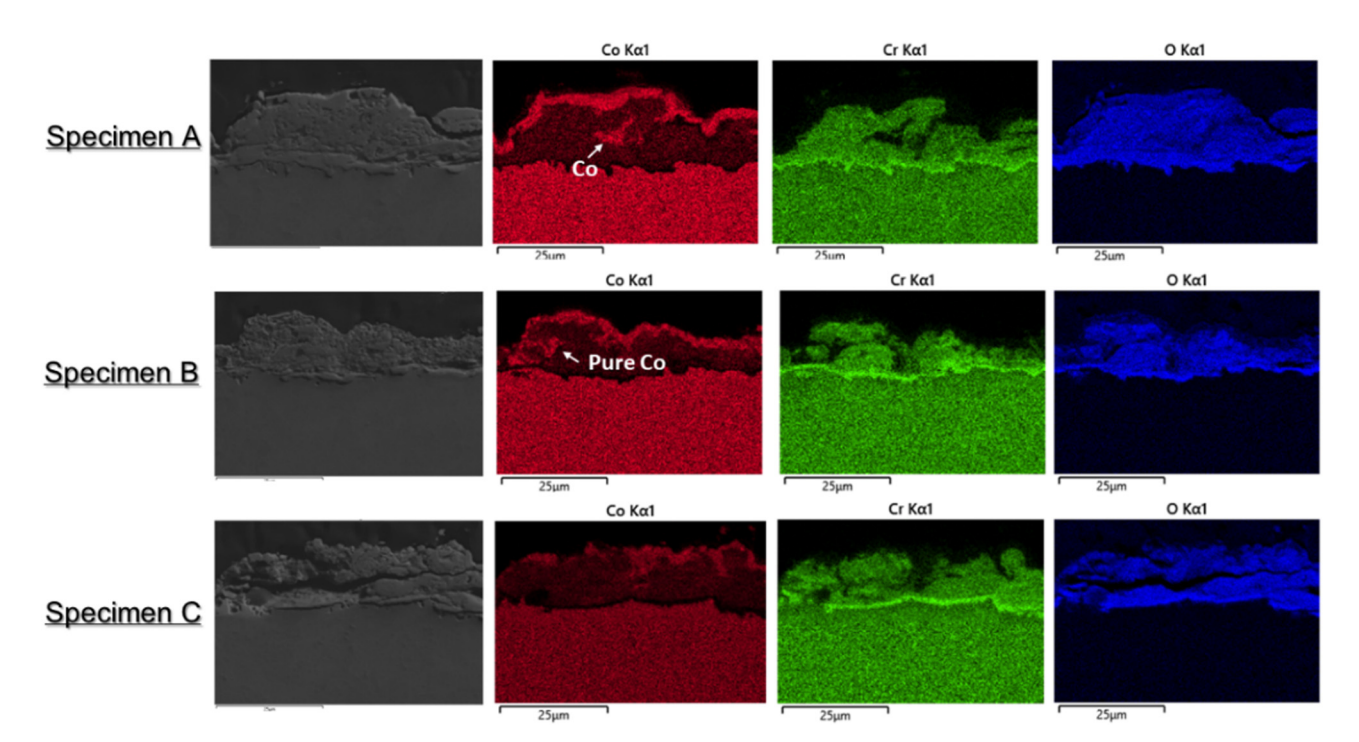


Figure 3: Cross-sectional SEM images and cartographies of Specimens A, B, and C.

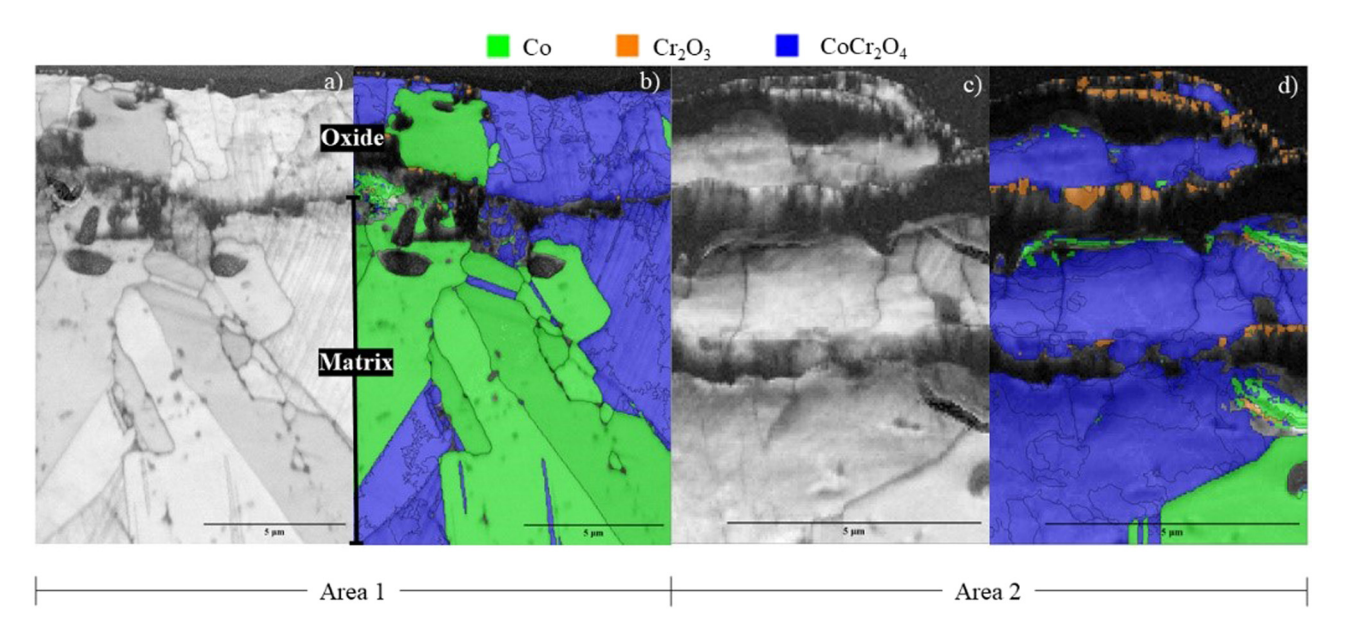


Figure 4: Cross-sectional EBSD images of Specimen C at two different areas: (a and b) for Area 1 showing both oxide scale and matrix and (c and d) for Area 2 showing only oxide.

3.3 Evolution of the specimen during oxidation

Figures 5–7 show the XRD patterns of Specimens A, B, and C, respectively, *in situ* characterised in air during the experiments and Table 3 shows the identification of the phases, comprising the Powder Diffraction Files number (PDF no.) reported by International Center for Diffraction

Data (ICDD), the crystal structure, and the lattice parameters, matched with XRD results. For Specimen A oxidised at 900°C, only the metallic Co (phase: Co-1) was observed at room temperature, pattern A1, confirming that there was no oxide before high temperature oxidation. The lattice parameter a and the cell volume of this phase were 3.569 Šand 45.453 ų. These were close to that reported by Saldivar-Garcia and Lopez [27] analysing the

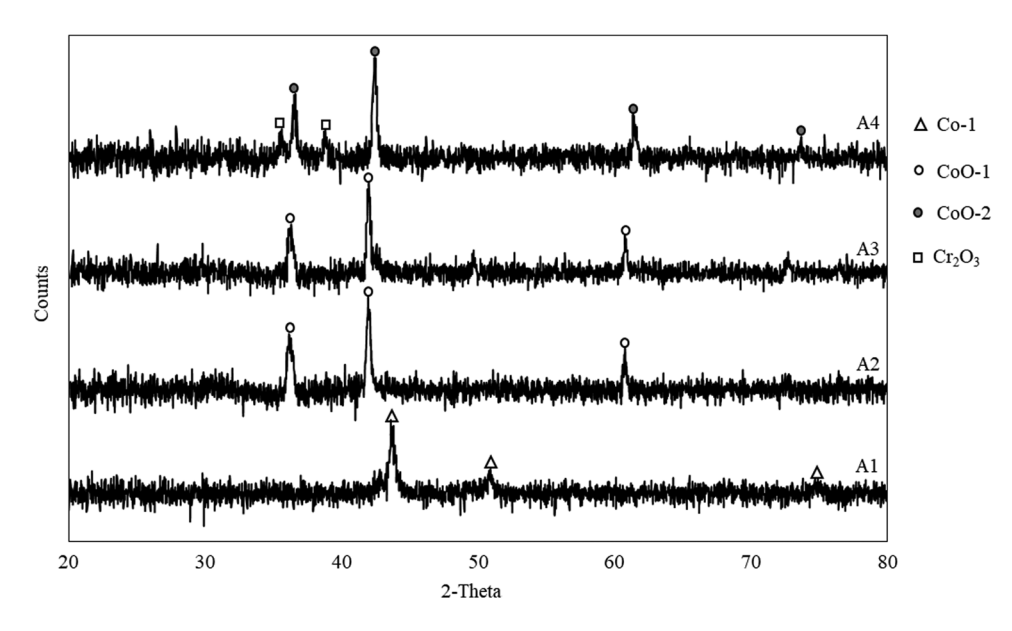


Figure 5: XRD pattern in the grazing incident mode of Specimen A oxidised in air at 900°C. The conditions where the characterisations were carried out were at 30°C (A1 pattern), after the temperature reached 900°C (A2 pattern), after holding at 900°C for 5 min (A3 pattern) and after cooling down the temperature to 50°C (A4 pattern).

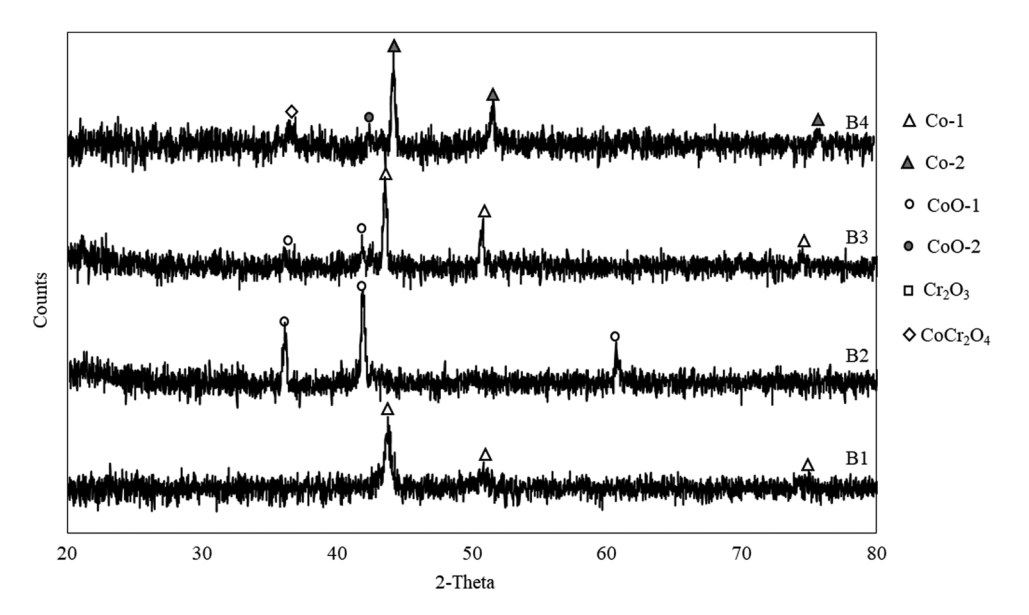


Figure 6: XRD pattern in grazing incident mode of Specimen B oxidised in air at 1,000°C. The conditions where the characterisations were carried out were at 30°C (B1 pattern), after the temperature reached 1,000°C (B2 pattern), after holding at 1,000°C for 5 min (B3 pattern), and after cooling down the temperature to 50°C (B4 pattern).

Co-27Cr-5Mo at room temperature and its lattice constant, a, was found to be 3.584 Å. After heating up to 900°C and holding at this temperature for a short period, CoO (phase CoO-1) was formed and fully covered on the specimen surface since the metallic Co cannot be observed anymore as shown in patterns A2 and A3. This CoO formation was proved by thermodynamic calculation that CoO was formed

during the oxidation of Co in the environment containing partial pressure of oxygen of 0.21 atm at 900°C [4,5]. After decreasing the temperature to 50°C, the pattern A4 shows the detection of both $\rm Cr_2O_3$ and CoO (phase CoO-2) with little shift of the peaks. Comparing the CoO-1 and CoO-2, they were both cubic structure with little difference in lattice parameters. The constant a and cell volume of CoO-1 were

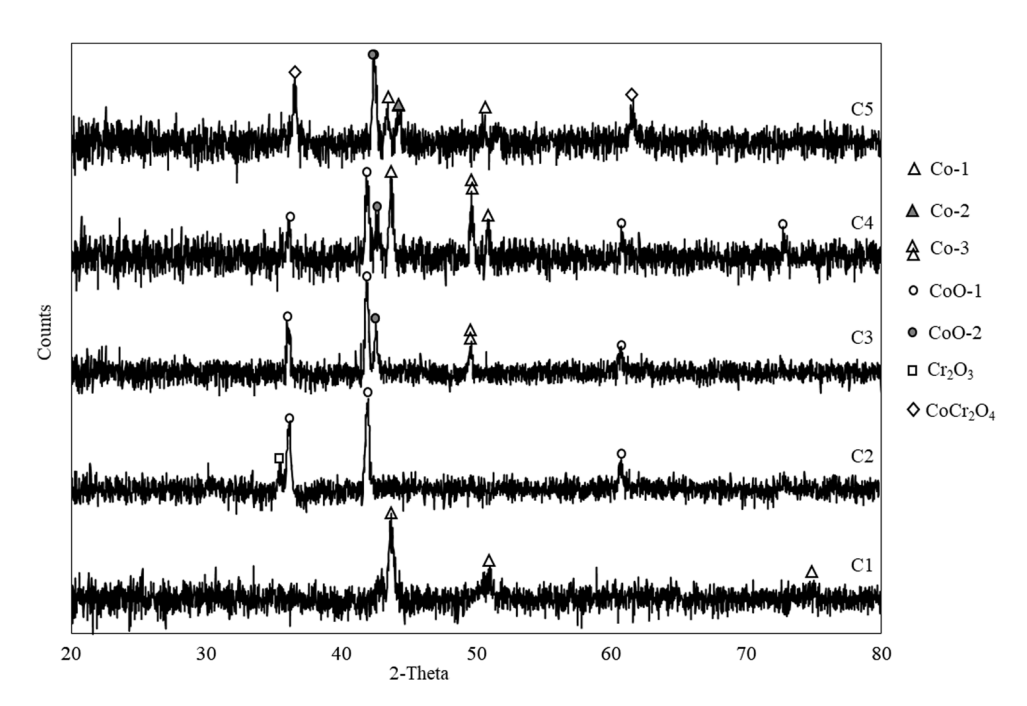


Figure 7: XRD pattern in grazing incident mode of Specimen C oxidised in air at 900 and 1,000°C, consequently. The conditions where the characterisations were carried out were at 50°C (C1 pattern), at 900°C during heating up (C2 pattern), at 1,000°C during heating up (C3 pattern), at 900°C during cooling down (C4 pattern), and after cooling down the temperature to 50°C (C5 pattern).

Table 3: Identification of all phases detected by XRD

| Phase | ICDD PDF no. | Crystal system | Lattice parameter | | | | | | |
|----------------------------------|--------------|----------------|-------------------|-------|--------|----|----|-----|----------|
| | | | a (Å) | b (Å) | c (Å) | α | β | у | Vol. (ų) |
| Co-1 | 01-071-4238 | Cubic | 3.569 | 3.569 | 3.569 | 90 | 90 | 90 | 45.453 |
| Co-2 | 01-077-7451 | Cubic | 3.544 | 3.544 | 3.544 | 90 | 90 | 90 | 44.524 |
| Co-3 | 04-015-9337 | Hexagonal | 2.514 | 2.514 | 4.105 | 90 | 90 | 120 | 22.524 |
| CoO-1 | 04-018-4843 | Cubic | 4.320 | 4.320 | 4.320 | 90 | 90 | 90 | 80.622 |
| CoO-2 | 01-078-0431 | Cubic | 4.260 | 4.260 | 4.260 | 90 | 90 | 90 | 77.418 |
| Cr_2O_3 | 01-082-3804 | Trigonal | 4.629 | 4.629 | 12.880 | 90 | 90 | 120 | 239.013 |
| CoCr ₂ O ₄ | 00-022-1084 | Cubic | 8.330 | 8.330 | 8.330 | 90 | 90 | 90 | 578.010 |

4.320 Å and 80.622 Å³, respectively, while those of CoO-2 were 4.260 Å and 77.418 Å³. It can be seen that the cell was smaller when the temperature reduced. This was because of the thermal expansion promoting the expansion of the cell at high temperatures [27]. The XRD pattern of Specimen A implied that Co was first oxidised forming CoO followed by the oxidation of Cr to form Cr2O3. This remark was confirmed by the work of Zimmermann et al. [28] finding that the initial oxide formed on CoCr alloy was Co-rich layer leaving the cation vacancies behind which allow the inward diffusion of O underneath the surface. Additionally, this revealed the counter transport of Co and O through the growing scale during high temperature oxidation [25]. This was the reason why CoO layer was formed externally as shown in Figure 3. Also, Ellingham diagram indicates that equilibrium partial pressure for the formation reactions of CoO and Cr₂O₃ at 900°C was about 5×10^{-13} and 5×10^{-25} atm respectively [7], so at the higher partial pressure of O2, 0.21 atm, in this study, these phases were ensured to be formed.

For Specimen B, no oxide was observed on the specimen before high temperature oxidation as shown in the pattern B1. After heating to 1,000°C, CoO (phase CoO-1) was first formed as in the pattern B2 which was similar to Specimen A. When the specimen was held at this temperature for a while, the intensity of CoO-1 was dropped while that of Co-1 which was the phase detected before oxidation became the main phase of the layer characterised. This implied the reformation of Co and confirmed the literatures [1,8,9] reporting that Co was able to form during high temperature oxidation as a product of CoO reduction, (equation (2)), if the partial pressure of O₂ in the scale was low. Therefore, this O production by reduction of CoO led to the further formation of Cr₂O₃ that was the reason why Cr₂O₃ was found to be the major oxide in the scale after long exposure time as observed by Li et al. [5]. No Cr₂O₃ peak was presented in this pattern. However, Figure 3 ensures the formation of Cr₂O₃. However, because the scale growth during the experiment increased the thickness of the oxide scale combined with the

analysis of very thin surface of the oxide layer, GI-XRD could not penetrate to the Cr₂O₃ layer where was at the oxide/alloy interface. After cooling down, the specimen surface was analysed again at 50°C and the results are shown the pattern B4. Due to the reduction in temperature, the shrinkages of the structures were appeared by CoO-2 and Co-2 phases identifying by their smaller lattice constants and cell volumes leading to replace the previous CoO-1 and Co-1 phases formed like occurring in Specimen A. Furthermore, CoCr₂O₄ was also observed in this pattern. These results together with FESEM, EDX, and EBSD were in good agreement with the research of Wright and Wood [29] oxidising Co-30Cr at 1,000°C. They demonstrated that the CoO was the outer layer, the Cr2O3 was the thin and partly continuous layer at the oxide/alloy interface while CoCr₂O₄ was between CoO and Cr₂O₃, and it was the major inner layer. In summary, what we observed from Specimens A and B can provide the sequence of the process as follows: (1) oxidation of Co to form CoO; (2) oxidation of Cr to form Cr₂O₃; (3) the reduction of CoO to form Cr₂O₃ and Co; and (4) the formation of (Co,Cr)₃O₄.

For Specimen C which was double-step oxidised at 900 and 1,000°C consequently, the metallic Co (phase Co-1) was the only phase detected before oxidation as same as what observed on Specimens A and B at room temperature. The pattern C2 exhibits the similar results to Specimens A and B that CoO-1 and Cr₂O₃ were formed during the beginning

Table 4: Chemical composition of Co-26Cr-6Mo alloy used in this work

| Material | Lati | tice para | Reference | |
|---|-------|-----------|-----------|-----------|
| | a (Å) | c (Å) | Vol (ų) | |
| Co-27Cr-6Mo | 2.514 | 4.105 | 22.524 | This work |
| Co-29.6Cr-7.4Fe-7.6Ni | 2.520 | 4.132 | _ | [30] |
| Co-27Cr-5Mo-0.05C | 2.541 | 4.099 | 22.920 | [27] |
| Co-28.5Mo-8.5Cr-2.6Si-3.0(Ni + Fe)-0.06C | 2.530 | 4.090 | 22.672 | [31] |
| Pure Co | 2.507 | 4.070 | 22.153 | [32] |

period of oxidation. The unusual but interesting result was found when the temperature reached 1,000°C as in pattern C3. The hexagonal Co (Co-3) was formed implying that the phase transition occurred. Saldivar-Garcia and Lopez [27] report that the temperature equilibrium of FCC and HCP structure of Co-27Cr-5Mo-0.05C alloy was around 970°C. Assuming that, due to rather similar composition of their alloy and the alloy used in this work, the phase transition equilibrium temperatures were approximately comparable. Taking into account the lattice constant, a, and the unit cell volume of hexagonal structure compared to that reported in the literatures [27,30–32] the parameters were rather closed, as shown in Table 4, ensuring that our Co-3 phase was actually HCP. In addition, CoO-1 and CoO-2 were detected at the same time. Gamarnick [33] described that the lattice parameters of the small particle can differ from that in a bulk crystal due to the excess or deficit of the inner stress called intracrystalline pressure as a result of the interaction between the elements of the charge lattice in the crystal. The energetic non-equivalence of the surface and inner cells specified the lattice parameter. It was possible that when the temperature increases, the intracrystalline pressure increases leading to the compression of the lattice; hence, the lattice parameters were smaller. Then, CoO-1 and CoO-2 were possible to be both found. After cooling to 900°C, the specimen was analysed again and the pattern C4 was attained. CoO-1 and CoO-2 can still be detected at this stage. Besides, the higher intensity of cubic Co-1 than that of the hexagonal Co-3 was found. As mentioned above, during the interchange between the temperature of 900 and 1,000°C, the FCC-HCP transition equilibrium temperature existed, so it might be at the step changing back into the FCC structure, then both phases were demonstrated. When the temperature was cooled down to 50°C, the final characterisation, pattern C5, the hexagonal Co-3 disappeared due to the temperature was much less than the transition temperature while both cubic forms of Co, Co-1 and Co-2, were found. The formation of Co-2 was probably due to the temperature drop and the composition variation in the oxide leading to develop the stress in the structure and then the lattice size was partly changed. CoO-1 was partly shrink and became CoO-2 like occurring Specimens B and C while the remaining reacted with Cr₂O₃ and form CoCr₂O₄.

4 Conclusions

(1). The reduction of CoO to promote O and metallic Co in the oxide scale was experimentally proved to occur consistent with thermodynamic calculation.

- (2). At the initial stage of oxidation, Co was the first element oxidised followed by Cr to form chromia.
- (3). The investigation of the oxide evolution revealed the oxidation reaction sequence occurring during high temperature oxidation.
- (4). The change in the lattice parameters due to the inner stress was observed especially when the temperature was cooling down to low temperature.
- (5). The hexagonal Co can also be observed at only high temperature around 900–1,000°C and it would disappear when the temperature became lower than this range.

Acknowledgments: The authors would like to thank Prof. Akihiko Chiba and Dr. Kenya Yamanaka from Institute for Materials Research, Tohoku University for providing the specimens of this research. In addition, Ms. Siriwan Ouampan from Thailand National Metal and Materials Technology Center (MTEC) is acknowledged for her helps and supports.

Fundig information: This research was funded by National Science, Research and Innovation Fund (NSRF) and King Mongkut's University of Technology North Bangkok with Contract no. KMUTNB-64-DRIVE-35.

Author contributions: Patthranit Wongpromrat: Conceptualization, Methodology, Validation, Formal analysis, Investigation, Resources, Data Curation, Writing — Original Draft, Writing — Review & Editing, Visualization, Project administration; Phacharaphon Tunthawiroon: Investigation; Eakarach Bumrungthaichaichan: Investigation; Phisan Ponpo: Investigation; Thanasak Nilsonthi: Validation, Formal analysis, Writing — Review & Editing, Funding acquisition; Somrerk Chandra-ambhorn: Validation, Formal analysis, Writing — Review & Editing, Supervision; Walairat Chandra-ambhorn: Validation, Formal analysis, Writing — Review & Editing.

Conflict of interest: Authors state no conflict of interest.

References

- [1] Coutsouradis, D., A. Davin, and M. Lamberigts. Cobalt-based superalloys for applications in gas turbines. *Materials Science and Engineering*, Vol. 88, 1987, pp. 11–19.
- [2] Makineni, S. K., A. Sharma, P. Pandey, and K. Chattopadhyay. An overview on Co-base alloys for high temperature applications. *Encyclopedia of materials: metals and alloy*, Elsevier, India, 2021.
- [3] Ye, Z., C. Li, Z. Huang, H. Luo, F. Chen, Z. Yan, et al. The effect of solution and aging treatments on the microstructure and mechanical properties of a selective laser melted CoCrMo alloy. *Journal of Materials Science*, Vol. 57, 2022, pp. 6445–6459.

[4] Zaman, H. A., S. Sharif, D. W. Kim, M. H. Idris, M. A. Suhaimi, and Z. Tumurkhuyaq. Machinability of cobalt-based and cobalt chromium molybdenum alloys - A review. Procedia Manufacturing, Vol. 11, 2017, pp. 563-570.

DE GRUYTER

- Li, Y., N. Tang, P. Tunthawiroon, Y. Koizumi, and A. Chiba. Characterisation of oxide films formed on Co-29Cr-6Mo alloy used in die-casting moulds for aluminium. Corrosion Science, Vol. 73, 2013. pp. 72-79.
- Li, Y., P. Tunthawiroon, N. Tang, H. Bian, F. Wang, S. Sun, et al. Effects of Al, Ti, and Zr doping on oxide film formation in Co-29Cr-6Mo alloy used as mould material for Al die-casting. Corrosion Science, Vol. 84, 2014, pp. 147-158.
- [7] Kofstad, P. K. and A. Z. Hed. Oxidation of Co-25 w/o Cr at high temperatures. Journal of the Electrochemical Society, Vol. 116, 1969, pp. 1542-1550.
- Kofstad, P. K. and A. Z. Hed. High-temperature oxidation of Co-10 w/o Cr alloys: I. microstructure of oxide scales. Journal of the Electrochemical Society, Vol. 116, 1969, pp. 224-149.
- Kofstad, P. K. and A. Z. Hed. High temperature oxidation of Co-10 w/o Cr alloys: II. Oxidation kinetics. Journal of the Electrochemical Society, Vol. 116, 1969, pp. 229-234.
- [10] Gorr, B., L. Wang, S. Burk, M. Azim, S. Majumdar, H. J. Christ, et al. High-temperature oxidation behavior of Mo-Si-B-based and Co-Re-Cr-based alloys. Intermetallics, Vol. 48, 2014, pp. 34-43.
- Klein, L., M. S. Killian, and S. Virtanen. The effect of nickel and silicon addition on some oxidation properties of novel Co-based high temperature alloys. Corrosion Science, Vol. 69, 2013, pp. 43-49.
- [12] Yeh, A. C., S. C. Wang, C. F. Cheng, Y. J. Chang, and S. C. Chang. Oxidation behaviour of Si-bearing Co-based alloys. Oxidation of Metals, Vol. 86, 2016, pp. 99-112.
- [13] Young, T. F., J. Kieffer, and G. Borchardt. Tracer diffusion of oxygen in CoO-SiO₂ melts. Journal of Physics: Condensed Matter, Vol. 6, 1994, pp. 9825-9834.
- [14] Wongpromrat, P., A. Galerie, T. Thublaor, W. Chandra-ambhorn, P. Ponpo, P. Watasuntornpong, et al. Evidence for chromium, cobalt and molybdenum volatilisations during high temperature oxidation of Co-27Cr-6Mo alloy. Corrosion Science, Vol. 202, 2022, id. 110285.
- Khan, A., Y. Huang, Z. Dong, and X. Peng. Effect of Cr₂O₃ nanoparticle dispersions on oxidation kinetics and phase transformation of thermally grown alumina on a nickel aluminide coating. Corrosion Science, Vol. 150, 2019, pp. 91-99.
- [16] Fu, G., L. Wei, X. Shan, X. Zhang, J. Ding, C. Lv, et al. Influence of a Cr₂O₃ glass coating on enhancing the oxidation resistance of 20MnSiNb structural steel. Surface and Coatings Technology, Vol. 294, 2016, pp. 8-14.
- [17] Sadeghi, E., N. Markocsan, and S. Joshi. Advances in corrosionresistant thermal spray coatings for renewable energy power plants. Part I: Effect of composition and microstructure. Journal of Thermal Spray Technology, Vol. 28, 2019, pp. 1749-1788.
- Sarrazin, P., A. Galerie, J. Fouletier. Mechanisms of high temperature corrosion: A kinetics approch. Trans Tech Publication, Switzerland, 2008.

- [19] Linder, M., T. Hocker, L. Holzer, K. A. Friedrich, B. Iwanschitz, A. Mai, et al. Cr₂O₃ scale growth rates on metallic interconnectors derived from 40,000 h solid oxide fuel cell stack operation. Journal of Power Sources, Vol. 243, 2013, pp. 508-518.
- Linder, M., T. Hocker, L. Holzer, K. A. Friedrich, B. Iwanschitz, A. Mai, et al. Oxide (Cr2O3) scale growth on metallic interconnects and its impact on ohmic resistance: Combined study of image analysis and modeling. 11th European SOFC & SOE Forum, Lucerne. Swtizerland: July 2014, pp. 1-4.
- [21] Opila, E. J., D. L. Myers, N. S. Jacobson, I. M. B. Nielsen, D. F. Johnson, J. K. Olminsky, et al. Theoretical and experimental investigation of the thermochemistry of CrO₂(OH)₂(q). Journal of Physical Chemistry A, Vol. 111, 2007, pp. 1971-1980.
- [22] Krumpelt, M., T. A. Cruse, B. J. Ingram, J. L. Roubort, S. Wang, P. A. Salvador, et al. The effect of chromium oxyhydroxide on solid oxide fuel cells. Journal of the Electrochemical Society, Vol. 157, 2010, pp. B228-B233.
- [23] Phalnikar, C. A., E. B. Evans, and W. M. Baldwin. High temperature scaling of cobalt-chromium alloys. Journal of the Electrochemical Society, Vol. 103, 1956, pp. 429-438.
- [24] Hou, G. Oxidation of a Co-base superalloy. Journal of Materials Science & Technology, Vol. 24, 2008, pp. 883-890.
- Weiser, M., R. J. Chater, B. A. Shollock, and S. Virtanen. Transport [25] mechanisms during the high-temperature oxidation of ternary y/y' Co-base model alloys. NPJ Materials Degradation, Vol. 3, 2019, pp. 1-11.
- [26] Przybylski, K. and D. Szwagierczak. Kinetics and mechanism of high-temperature oxidation of dilute cobalt-chromium alloys. Oxidation of Metals, Vol. 17, 1982, pp. 267-295.
- Saldivar-Garcia, A. J. and H. F. Lopez. Temperature effects on the lattice constants and crystal structure of a Co-27Cr-5Mo low-carbon alloy. Metallurgical and Materials Transactions A: Physical Metallurgy and Materials Science, Vol. 35A, 2004, pp. 2517-2523.
- [28] Zimmermann, J. and L. C. Ciacchi. Original and the selective Cr oxidation in CoCr alloy surfaces. Journal of Physical Chemistry Letters, Vol. 1, 2010, pp. 2343-2348.
- [29] Wright, I. G. and G. C. Wood. The isothermal oxidation of Co-Cr alloys in 760 torr oxygen at 1000°C. Oxidation of Metals, Vol. 11, 1977, pp. 163-191.
- [30] Wang, W., Z. Hou, R. Lizrraga, Y. Tian, R. P. Babu, E. Holmstrom, et al. An experimental and theoretical study of duplex fccbhcp cobalt based entropic alloys. Acta Materialia, Vol. 176, 2019, pp. 11-18.
- [31] Halstead, A. and R. D. Rawlings. Structure and hardness of Co-Mo-Cr-Si wear resistant alloys (Tribaloys). Metrials Science, Vol. 18, 1984, pp. 491-500.
- [32] Taylor, A. and R. W. Floyd. Precision measurements of lattice parameters of non-cubic crystals. Acta Crystallographica, Vol. 3, 1950, pp. 285-289.
- [33] Gamarnik, M. Y. The physical nature of changes of lattice parameters in small particles. Physica Status Solidi (B), Vol. 178, 1993, pp. 59-69.